An Electromagnetic Imaging Algorithm Based on Generative Adversarial Network for Limited Observation Angle

Chun Xia Yang[1], Xirui Yang[1, 2], Jian Zhang[3], Chi Zhou[1], and Mei Song Tong[4]

[1]Shanghai Engineering Research Center of Intelligent Education and Bigdata
Shanghai Normal University, Shanghai 200234, China
chunxiay@shnu.edu.cn, 1000448084@smail.shnu.edu.cn, 1000528179@smail.shnu.edu.cn

[2]School of Electronic and Information Engineering
Guangzhou City University of Technology, Guangzhou 510800, China

[3]Xpeedic Technology, Inc.
Shanghai 201210, China
jian.zhang@xpeedic.com

[4]Department of Electronic Science and Technology
Tongji University, Shanghai 201804, China
mstong@tongji.edu.cn

***Abstract* –** In the context of long-distance detection and obstacle occlusion, the limited observation angle of electromagnetic imaging poses significant challenges for accurate reconstruction. To address this issue, we propose a hybrid electromagnetic reconstruction algorithm based on a generative adversarial network (GAN). This algorithm utilizes the diffraction tomography (DT) method to generate an initial image, which serves as input for the GAN. Through adversarial training between the generator and the discriminator, the algorithm produces a reconstructed image with enhanced accuracy. Firstly, unlike complete learning-based reconstruction methods that rely solely on scattering field data, our approach effectively integrates both scattering characteristics and *a priori* information from the DT image model, thus improving the accuracy and generalizability of the neural network. Secondly, compared to other linear approximation algorithms, the DT algorithm incorporates fast Fourier transform (FFT) to enhance computational efficiency. Thirdly, this study employs a Fourier spatial data extrapolation technique to mitigate the limitations of insufficient data and improve imaging fidelity. Numerical simulations demonstrate that even at a narrow observation angle of 90°, the proposed algorithm exhibits excellent reconstruction performance and notable generalization ability.

***Index Terms* –** diffraction tomography (DT), generative adversarial network (GAN), inverse scattering, limited angle.

I. INTRODUCTION

In recent years, with the rapid development of artificial intelligence, deep learning technology has made great progress in the electromagnetic field [1, 2], which is expected to bring new ideas for solving inverse scattering problems. Using deep learning to solve electromagnetic inverse problems, the direct approach is to take the measured scattering data as input of the neural network and output the detected target image, which is called complete learning or direct learning reconstruction [3]. In the complete learning reconstruction, neural networks basically operate as a black box, with the user's workload being minimal while the neural network undertakes a heavy task. Due to the unnecessary computational cost spent on learning known physical models or laws, only very simple scatterers can usually be reconstructed.

Recent advancements indicate that the integration of physics-based and data-driven methodologies can substantially improve the analysis and prediction of complex systems. A prominent strategy involves addressing the inverse scattering problem by incorporating deep learning as a complementary computational tool within the framework of traditional physics-based methods. For instance, Guo et al. [4] employed the supervised descent method to solve a two-dimensional microwave imaging challenge. They utilized a neural network to learn the average descent direction between the initial and target models, thereby accelerating model updates and avoiding computationally intensive partial derivative calculations. This approach not only streamlines the

Submitted On: January 15, 2025
Accepted On: July 31, 2025

https://doi.org/10.13052/2025.ACES.J.400803

process but also substantially reduces overall computational costs compared to conventional non-learning algorithms. Another effective strategy is to leverage deep learning techniques to generate an initial estimate for the traditional electromagnetic inverse scattering model. Chen et al. [5] trained a convolutional neural network (CNN) to learn a complex mapping function from magnetic resonance T1 images to dielectric property images. The dielectric image generated by this CNN serves as the initial estimate for microwave imaging, which is then refined through a physics-based image processing step. Similarly, Sanghvi et al. [6] used the signal subspace component of the total contrast source as input to train a CNN, obtaining an initial estimate of the total contrast source. This estimate is subsequently refined using traditional iterative optimization techniques.

Additionally, another strategy takes data-driven methods as the main imaging approach, in which the input data, labels, loss functions, and neural network structures are designed based on physical laws [7]. Some scholars propose a two-step inversion strategy that combines traditional electromagnetic imaging algorithms with neural networks [8, 9]. From a computational efficiency perspective, linear approximation inversion algorithms are commonly employed, where the preliminary imaging results serve as inputs for the neural network instead of scattering data [10, 11]. This approach significantly reduces the learning complexity of the network [12, 13].

While deep learning holds significant potential for electromagnetic inverse scattering, its practical application encounters several critical challenges: (1) Data scarcity: Collecting adequate high-precision scattering field data in real-world scenarios is both expensive and resource-intensive, and the limited availability of observation angles further compounds this issue; (2) Model generalizability: Purely data-driven approaches are prone to overfitting to the training data distribution, which limits their adaptability to complex targets or non-ideal conditions; (3) Physical consistency: Black-box models may produce solutions that contradict fundamental electromagnetic principles, resulting in physically implausible outcomes.

Traditional physics-based methods, such as diffraction tomography (DT) [14, 15], establish explicit mappings between scattering fields and target parameters through Fourier transforms and linear approximations. Despite being constrained by limited observation angles and approximation inaccuracies, these methods offer physically meaningful constraints and computationally efficient initial estimates. In our hybrid physics-data-driven framework, the physical priors of DT are integrated into GAN [16, 17] training to effectively tackle the aforementioned challenges. Specifically, DT's low-complexity initial estimates alleviate the learning burden on the network, while Fourier-based data extrapolation [18] augmented with prior knowledge mitigates data insufficiency. Furthermore, adversarial training improves both generalizability and physical consistency.

This paper is organized as follows: Section II introduces the physical model and formulation of the inverse scattering problem. In Section III, we present a hybrid reconstruction algorithm based on GAN. Section IV provides numerical and experimental results along with their analyses. Finally, Section V summarizes the conclusions.

II. THE ELECTROMAGNETIC INVERSE SCATTERING PROBLEM

Consider a two-dimensional electromagnetic inverse scattering problem. As illustrated in Fig. 1, DOI represents an imaging region in free space containing an unknown scatterer that needs to be detected. The transmitting antenna, located in the observation region S, emits electromagnetic waves to illuminate the imaging region DOI. This induces currents on the scatterer, generating scattered fields. The receiving antennas measure the scattered fields. Then the electromagnetic parameter distribution in imaging region is calculated by inversion algorithms, and the target's spatial position, contour, and internal structure are reconstructed. Assuming that the permeability of the unknown scatterer is the same as the background medium, the objective of reconstruction is the distribution of the relative permittivity in the imaging region.

The scattering integral equation is shown as follows:

$$E^{\mathrm{tot}}(\rho) = E^{\mathrm{inc}}(\rho) + k_b{}^2 \int_{\mathrm{DOI}} g(\rho,\rho') \cdot O(\rho') E^{\mathrm{tot}}(\rho') \mathrm{d}\rho', \rho \in \mathrm{S} \quad (1)$$

where ρ represents the position of the receiving antenna, ρ' represents the position of any point in the imaging region. $g(\rho,\rho') = \frac{i}{4} H_0^{(1)}(k_b|\rho-\rho'|)$ is the two-dimensional Green's function in free space where $H_0^{(1)}$ is the zeroth order Hankel's function of the first kind and k_b is the wavenumber of the background medium. $O(\rho') = \varepsilon_r(\rho') - 1$ represents the contrast distribution, $E^{\mathrm{tot}}(\rho)$ represents the total field, $E^{\mathrm{inc}}(\rho)$ represents the incident field, and the integral term corresponds to the scattered field $E^{\mathrm{sca}}(\rho)$.

III. THE HYBRID RECONSTRUCTION ALGORITHM BASED ON GAN

A. Diffraction Tomography

In Eq.(1), the total field equals the superposition of the incident field and the scattered field. When the scattered field is much weaker relative to the incident field, the incident field can be used to approximate the total field according to the first-order Born approximation. Furthermore, assuming that both the transmitting

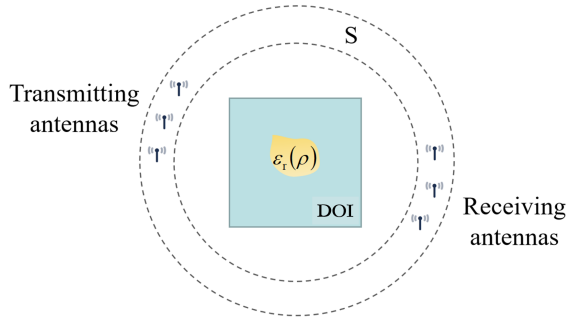

Fig. 1. Electromagnetic inverse scattering model.

antenna and the receiving antenna are located in the far field region of DOI, after a series of derivations, the scattered field can be expressed as [19]:

$$E^{\mathrm{sca}}(\rho_T,\rho_R) \simeq \frac{ik_b}{8\pi\sqrt{|\rho_T||\rho_R|}} e^{ik_b(|\rho_T|+|\rho_R|)} \int_{\mathrm{DOI}} e^{-i(k_b(\hat{\rho}_T+\hat{\rho}_R))\rho'} \cdot O(\rho') d\rho' , \quad (2)$$

where $E^{\mathrm{sca}}(\rho_T,\rho_R)$ denotes the scattered field detected by the receiver located at position vector ρ_R, which is generated by the transmitter situated at position vector ρ_T. $\hat{\rho}_T$ and $\hat{\rho}_R$ represent unit vectors in the ρ_T and ρ_R directions, respectively.

Eq. (2) is the formula of the DT algorithm, where the term on the right-hand side conforms to the form of a Fourier transform. Therefore, after measuring the scattering field data at the observation points, the contrast distribution can be obtained by applying simple coefficient multiplication and inverse Fourier transform. Discretizing the imaging region into N pixels, the computational cost of DT is only $O(NlogN)$. The computational complexity of other linear inversion approaches such as the backpropagation method (BP) is $O(N_{inc}N_fNlogN)$ [20, 21], where N_{inc} is the number of incidences, and N_f is the number of iterations for solving the forward problem.

B. Data Extrapolation Based on Fourier Transform

The practical realization of an optimal antenna configuration for achieving comprehensive coverage around the imaging area poses substantial engineering challenges. The restricted viewing angle range reduces diversity in scattering data, posing a challenge for precise reconstruction. To address these challenges, this study integrates a Fourier transform-based extrapolation method, incorporating *a priori* knowledge, to infer missing data in addition to the conventional DT algorithm, thereby enhancing the accuracy and reliability of the results. The following is a concise overview of the steps for implementation, with comprehensive details provided in reference [18].

For convenience, the equation (2) is abbreviated as

$$E(\rho) \simeq \mathscr{F}(O(\rho')), \quad \rho \in \mathrm{S}, \quad \rho' \in \mathrm{DOI}. \quad (3)$$

The limitation of the observation angle results in only a restricted segment of $E(\rho)$ being measurable, which is denoted as

$$E_1(\rho) = E(\rho)g(\rho),$$
$$\text{where } g(\rho) = \begin{cases} 1, & \rho \in \text{known area}, \\ 0, & \text{otherwise}. \end{cases} \quad (4)$$

Step 1: The contrast distribution in the imaging space is obtained by inverse Fourier transform of the scattering data.

$$O_n(\rho') = \mathscr{F}^{-1}(E_n(\rho)), \quad (5)$$

where $\mathscr{F}^{-1}$ is the inverse operator of $\mathscr{F}$.

Step 2: The target distribution is updated by adjusting the contrast values obtained in the previous step based on *a priori* information.

$$\widetilde{O}_n(\rho') = \begin{cases} O_n(\rho'), & \text{if } O_n(\rho') > 0 \\ 0, & \text{otherwise} \end{cases}. \quad (6)$$

Step 3: The updated contrast data is transformed by the operator $\mathscr{F}$ to obtain the corresponding scattering data.

$$\widetilde{E}_n(\rho) = \mathscr{F}(\widetilde{O}_n(\rho')). \quad (7)$$

Step 4: The initial measurement data is employed for local recovery of the previously updated scattering data.

$$E_{n+1}(\rho) = \widetilde{E}_n(\rho) + \left[E_1(\rho) - \widetilde{E}_n(\rho)\right] g(\rho) = \begin{cases} E_1(\rho), & \rho \in \text{known area} \\ \widetilde{E}_n(\rho), & \text{otherwise} \end{cases}. \quad (8)$$

Step 5: When the termination condition is met, the iteration ends; otherwise, return to Step 1 and increase n by 1. By iteratively following these steps, it becomes feasible to preserve the original measurement data while gradually inferring missing data, thereby significantly enhancing the quality of target reconstruction. The effective contrast range for numerical simulation is defined as $[0,\infty)$ in this study aligning with the typical parameters commonly employed in inverse scattering problems. For practical engineering scenarios, more sophisticated prior conditions can be specified.

The Fourier extrapolation enhances reconstruction accuracy through two key mechanisms. First, Fourier-domain completion. Under limited observation angles, the measurable scattering data corresponds to a truncated segment of the target's Fourier spectrum. By iteratively applying prior constraints (e.g., non-negativity of contrast, spatial sparsity) during extrapolation, we infer missing high-frequency components (as described in Eq. (8)). This process mitigates artifacts and refines edges in the DT image, providing higher-quality inputs for the GAN. Second, physical consistency enforcement. The iterative updates outlined in Eqs. (6)–(8) ensure

that the extrapolated data are consistent with both the measured scattering fields and prior knowledge (e.g. expected permittivity ranges). This approach suppresses non-physical oscillations in the reconstructed image, which are commonly encountered in purely data-driven methods under sparse measurement conditions.

C. Generative Adversarial Network

In this paper, we utilize the GAN as the network model for the data-driven component of the hybrid inversion algorithm. The GAN framework comprises two key components: a generator and a discriminator [22]. The unique adversarial training mechanism allows the model to more effectively capture complex data features and generate high-precision images, making it especially suitable for addressing the inverse scattering problem discussed in this paper. However, traditional purely data-driven GANs face challenges in handling missing data under limited observation angles and may produce non-physical solutions. Our algorithm incorporates physical constraints through DT initialization and Fourier-space extrapolation. Firstly, DT's linear approximations efficiently generate initial target estimates, avoiding direct learning of complex scattering mappings. Secondly, extrapolation utilizes prior knowledge (e.g., target contrast range, spatial sparsity) to constrain solution spaces and suppress non-physical outputs. Finally, the U-Net generator retains the low-frequency features of DT via skip connections, while the Convolutional Block Attention Module (CBAM) [23] module enhances edge reconstruction, thereby ensuring synergistic optimization of physical principles and data-driven features.

1) Generator. The structures of the generator and discriminator networks are illustrated in Fig. 2. In this work, the generator model adopts the structure of U-Net [24]. U-Net is a convolutional neural network commonly used for image segmentation. It has a U-shaped structure consisting of a symmetric encoder and decoder. The encoding part encodes the input rough image through a sequence of convolutional layers to obtain higher-dimensional feature representations. The decoding part decodes the latent space vector through a series of upsampling to reconstruct an image resembling the training data eventually. The feature maps of corresponding dimensions in the downsampling and upsampling processes are fused by employing the skip connection structure. In this paper, during each downsampling process, the CBAM is incorporated to enhance the representation capability of the generator network. This is achieved by selectively emphasizing informative features while suppressing irrelevant ones. The reconstruction accuracy of the relative permittivity and position of the target scatterer is further improved.

2) Discriminator. Compared with other network architectures, the GAN stands out due to its incorporation of a discriminator. The discriminator network contains several convolutional layers and finally passes through an average pooling layer followed by a sigmoid activation operation. In this study, the discriminator receives two distinct types of input data: one consists of real images from the training set, which represent the true distribution of scatterers; the other comprises synthetic images generated by the generator G. The discriminator's role is to estimate the probability that an input

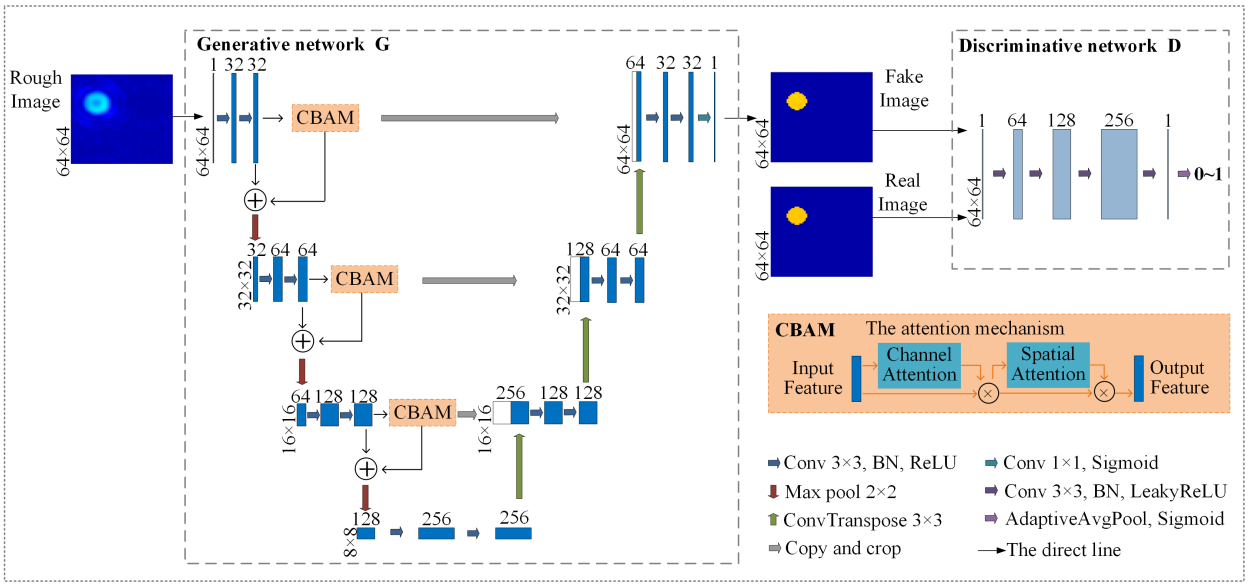

Fig. 2. The structure of the GAN.

sample originates from the training data rather than from the generator, thereby assessing the authenticity of the generated samples and providing feedback to the generator. This feedback mechanism prompts the generator to iteratively refine its parameters to produce increasingly realistic samples.

3) Training process. The generator and discriminator are trained in an adversarial manner until a Nash equilibrium is reached. This can be mathematically described as:

$$\min_{\theta_{\mathrm{G}}}\max_{\theta_{\mathrm{D}}} V(\theta_{\mathrm{G}},\theta_{\mathrm{D}}) = \mathbb{E}_{I^{real}\sim P_{real}(I^{real})}[\log \mathrm{D}_{\theta_{\mathrm{D}}}(I^{real})] + \mathbb{E}_{I^{rough}\sim P_{rough}(I^{rough})}[\log(1-\mathrm{D}_{\theta_{\mathrm{D}}}(\mathrm{G}_{\theta_{\mathrm{G}}}(I^{rough})))]. \tag{9}$$

Here, $\mathbb{E}$ denotes the mathematical expectation of the data distribution, I^{real} represents the real image, I^{rough} denotes the rough image input to the generator, while θ_{G} and θ_{D} refer to parameters to be trained in the generator and discriminator, respectively.

The loss function for the generator is defined as:

$$L_{\mathrm{G}} = \alpha L_{\mathrm{GAN}}^{\mathrm{G}} + L_{\mathrm{MSE}}. \tag{10}$$

The first term on the right-hand side of the equation represents the adversarial loss, where α serves as a weighting parameter, and L_{MSE} denotes the pixel-wise mean square error between the generated image and the real image distribution. The specific formula is as follows:

$$L_{\mathrm{MSE}} = \frac{1}{N}\sum_{i=1}^{N}\left(I_{\rho_i}^{real} - \mathrm{G}_{\theta_{\mathrm{G}}}(I^{rough})_{\rho_i}\right)^2. \tag{11}$$

In this paper, the generator is pre-trained using L_{MSE} prior to adversarial training in order to accelerate the learning process and prevent convergence to local optima. The adversarial loss is defined as:

$$L_{\mathrm{GAN}}^{\mathrm{G}} = -\log\left(\mathrm{D}_{\theta_{\mathrm{D}}}\left(\mathrm{G}_{\theta_{\mathrm{G}}}(I^{\mathrm{Rough}})\right)\right). \tag{12}$$

This equation indicates that the control parameters θ_{D} of the discriminator remains constant, while the parameters θ_{G} of the generator is optimized to enable the output image to deceive the discriminator to the greatest extent possible.

Similarly, when the generator parameters θ_{G} are held constant, training the discriminator parameters θ_{D} enhances its ability to accurately differentiate between real and generated images. Throughout this adversarial training process, the discriminator's ability to discern between real and synthetic samples also progressively improves. Ultimately, the model converges to an equilibrium where the generator produces samples so realistic that the discriminator can no longer reliably distinguish between real and generated data.

IV. NUMERICAL ANALYSIS

A. Test One: Circular Scatterers

The simulation setup is defined as follows. The imaging area is a square with each side measuring 0.8 m, divided into a grid of 64×64 pixels. The center of the imaging area serves as the coordinate origin. The observation area is equipped with 17 transmitting antennas and 17 receiving antennas, uniformly distributed along an arc spanning from 0° to 90°, with a radius of 2 m from the origin. Each transmitting antenna successively emits incident waves containing three frequencies (that is, 0.5 GHz, 1.0 GHz and 1.5 GHz) to illuminate the imaging area. Meanwhile, all receiving antennas synchronously capture the scattered fields generated by each individual incident wave.

The target is a circular homogeneous dielectric with a relative permittivity ranging from 1.2 to 3 (contrast of 0.2 to 2 with a step size of 0.1) and a radius range between 0.03 m and 0.08 m (with a step size of 0.01 m). The center coordinates are distributed within the range $(-0.2$ to $0.2, -0.2$ to $0.2)$ m. 3000 sets of training data and 300 sets of testing data were generated via simulation using the Method of Moments (MoM). The GAN adopts the Adam optimizer with $\beta_1 = 0.9$ and $\beta_2 = 0.999$. The learning rates for the generator and discriminator are both set to 1×10^{-5}. The batch size is set to 8, and the training process has been conducted for 200 epochs. The adversarial loss parameter α is set to 1×10^{-3}. The setting of these hyperparameters was guided by relevant literature [22][24], and their optimal values were identified through systematic numerical experiments.

By comparing the simulation results with the GAN-based direct inversion algorithm (referred to as "GAN") and the hybrid algorithm combining BP and GAN (referred to as "BP+GAN"), we validate the performance of the proposed hybrid electromagnetic reconstruction algorithm that combines extrapolated enhanced DT and GAN (referred to as "DT+GAN"). Specifically, the GAN algorithm utilizes scattered field data directly, whereas BP+GAN uses images reconstructed by the BP algorithm as input for its neural network. The results are presented in Fig. 3, where the first column displays the test sample with a radius of 0.04 m and a contrast value of 1.1. Meanwhile, the second column exhibits the sample with a radius of 0.07 m and a contrast value of 0.8. The hybrid inversion methods exhibit a superior capability in differentiating scatterers from the background, significantly outperforming the direct learning reconstruction method. In particular, the DT+GAN method achieves a more precise reconstruction of contrast values compared to the BP+GAN approach.

To quantify the reconstruction accuracy, the imaging error is calculated using the following formula[25]:

$$error = \frac{100\%}{N}\frac{\sum_{n=1}^{N}\left|\widetilde{O}(\rho)-O(\rho)\right|^2}{\sum_{n=1}^{N}|O(\rho)|^2}. \tag{13}$$

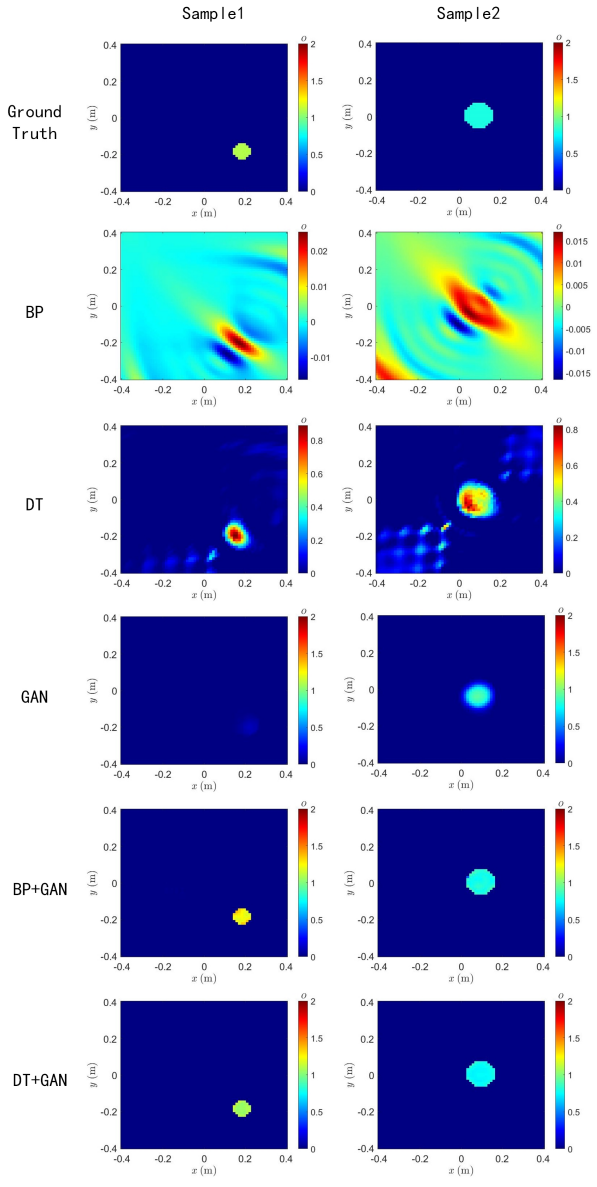

Fig. 3. The reconstruction results of a single circle under $0^\circ - 90^\circ$ observation. The first row illustrates the ground truth distribution, while the second, third, fourth, fifth, and sixth rows depict the reconstruction results of BP, DT, direct GAN, BP+GAN, and DT+GAN respectively.

The contrast of a cell in the imaging region predicted by the neural network is denoted as $\tilde{O}(\rho)$, while $O(\rho)$ represents the actual contrast of the corresponding position. Here, N refers to the number of cells in the imaging region. The cumulative distribution functions (CDFs) of the inversion error of BP+GAN and DT+GAN in the test set are shown in Fig. 4. The average reconstruction error for BP+GAN is $4.63 \times 10^{-6}\%$, while for DT+GAN it is $2.54 \times 10^{-6}\%$.

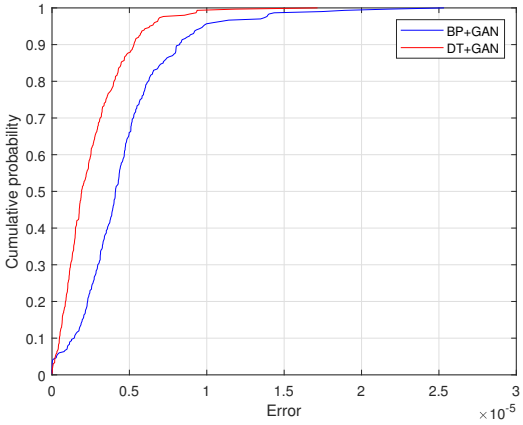

Fig. 4. CDFs of the reconstruction error for a single circular object.

The average execution times for the components BP, DT and GAN in hybrid algorithms based on 300 test samples have been analyzed. The BP algorithm recorded an average execution time of 0.0749 s, while the DT algorithm was significantly faster at 0.0050 s. The GAN component, when integrated with both BP and DT in the hybrid algorithms (BP+GAN and DT+GAN), demonstrated an average processing time of 0.2357 s, with negligible variation across different configurations. The execution time is measured on a computer equipped with an Intel i5-12400F CPU and an NVIDIA GeForce RTX 4060 GPU. These results highlight the superior computational efficiency of the DT algorithm compared to BP, even when an extrapolation step is included. The difference in solution efficiency can be attributed to the fact that the computation time of the BP algorithm increases significantly with the increase in the number of excitation waves, while this factor has a relatively minor impact on the DT algorithm.

To assess the generalization capability of the inversion algorithms, two dielectric circles were employed as reconstruction targets to evaluate the above neural networks. By testing 300 randomly generated samples, the BP+GAN model achieves an average error of $5.90 \times 10^{-3}\%$, whereas the DT+GAN model achieves an average error of $5.20 \times 10^{-3}\%$. Fig. 5 illustrates the reconstruction results for two samples, while Fig. 6 plots the CDFs of the reconstruction errors. In Sample 1, the contrast values of the two circles are set to 1.6 and 0.4, with corresponding radii of 0.03 m and 0.05 m, respectively. In Sample 2, the contrast values are adjusted to 0.2 and 0.7, with corresponding radii of 0.03 m and 0.06 m, respectively. The simulation results demonstrate that both direct GAN and BP+GAN tend to lose information regarding the target with low contrast during the reconstruction of the two-circle target,

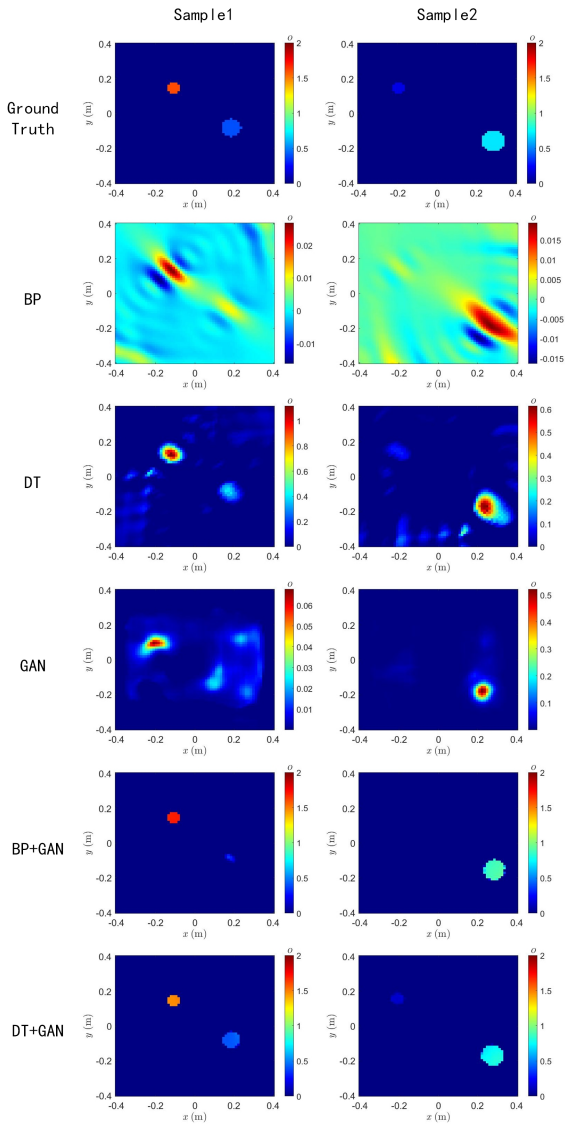

Fig. 5. Reconstruction results of two circular structures in the test of generalization ability.

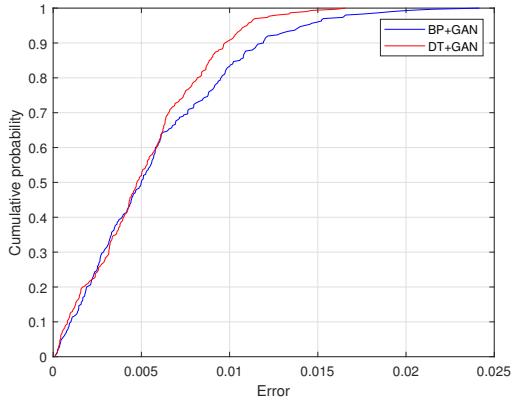

Fig. 6. CDFs of two circle reconstruction errors used to evaluate generalization ability.

whereas DT+GAN does not exhibit this issue. Although there is a slight deviation in capturing scatterer structure details, DT+GAN successfully achieves accurate inversion of both the target location and contrast value.

B. Test Two: Handwriting Digits

In this section, the reconstruction target is derived from the MNIST dataset [26], a widely utilized database of handwritten digits in the field of machine learning. The scatterers are modeled as dielectric materials with randomly assigned relative permittivities ranging between 1.2 and 3.0. Each image is upscaled from its original size of 28×28 pixels to 64×64 pixels to align the spatial resolution with the imaging setup described in Section IV-A. This adjustment standardizes the problem scale across tests and increases the number of unknowns, thereby intensifying the complexity of the inverse problem. Such a practice enables robust comparisons of reconstruction fidelity under heightened computational demands. The imaging model and neural network parameters were set identical to those used in test one. A simulation employing the MOM generated a training set consisting of $10,000$ samples, along with a validation set of $1,000$ samples and a testing set of 300 samples. Fig. 7 presents reconstructed profiles from two representative examples, while Fig. 8 displays the CDFs of the reconstruction errors. Since both BP and DT are linear approximate inversion algorithms, and given the large training dataset used in this experiment, the difference in reconstruction quality between the BP+GAN model and the DT+GAN model is not pronounced.

To evaluate the generalization performance of the algorithms, a randomly distributed circular scatterer is introduced into the imaging region, following the settings from test one, which may cause partial occlusion of the handwritten digits. Fig. 9 displays images of two reconstructed samples, whereas Fig. 10 illustrates the CDFs of the reconstruction errors. The results indicate that, compared to BP+GAN, DT+GAN demonstrates superior generalization capability, allowing for better differentiation of distinct targets within the imaging region and achieving a reconstructed contrast value that is more closely aligned with the ground truth.

C. Test Three: Experimental Data

In this section, we validate the proposed reconstruction method using experimental data provided by the Fresnel Institute. The measurement system is detailed in reference [27]. The scatterer is an off-centered circular cylinder with a significant vertical dimension, presenting an almost two-dimensional structure. Slightly deviating from the previous simulation model, the transmitter remains fixed while the scatterer rotates about the central vertical axis from 0° to 350° in increments of 10°. To assess the reconstruction performance

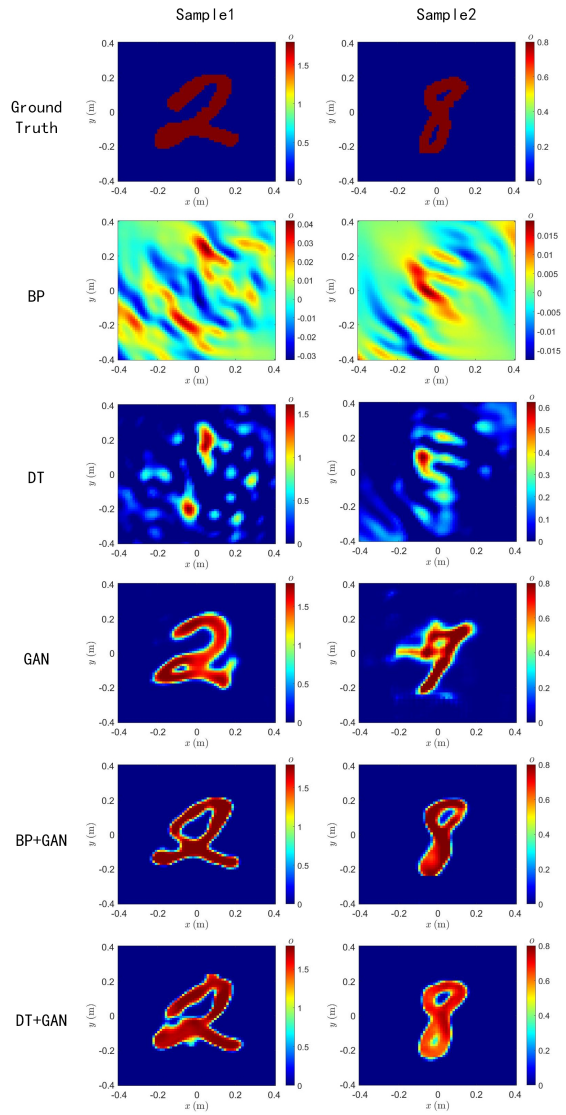

Fig. 7. The reconstructed results of handwritten digits from MNIST database.

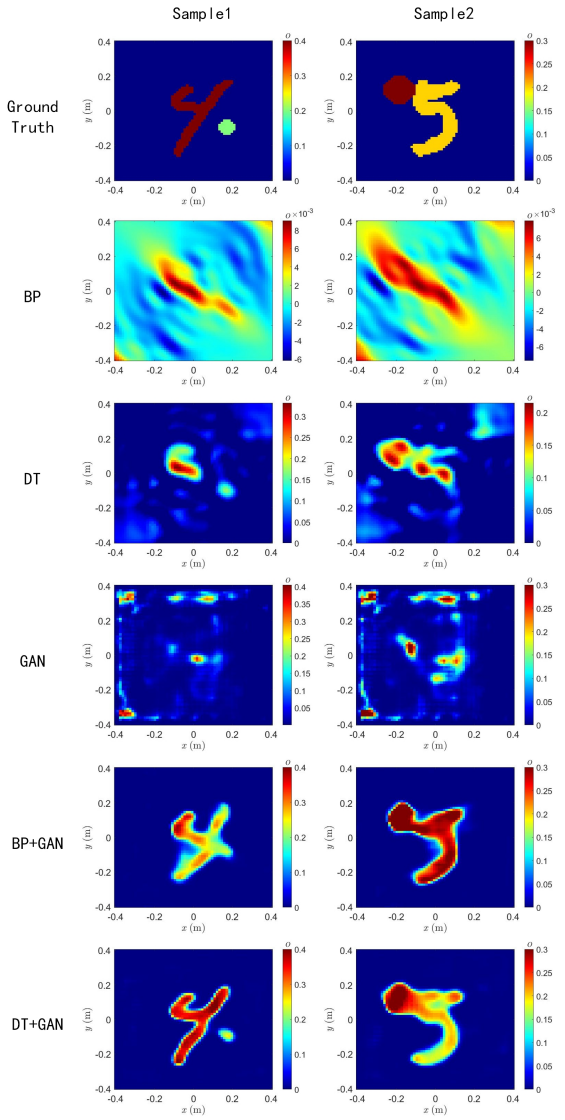

Fig. 9. The reconstructed results of handwritten digits with an extra circle.

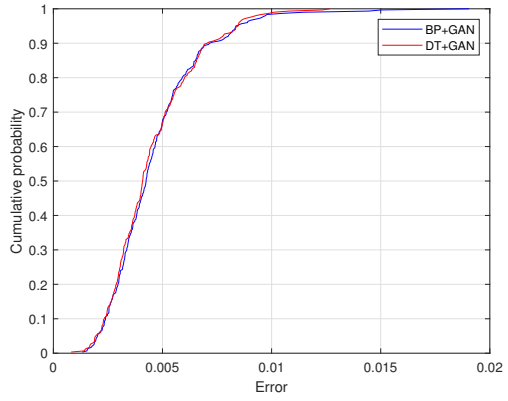

Fig. 8. CDFs of the reconstruction error for handwritten digits.

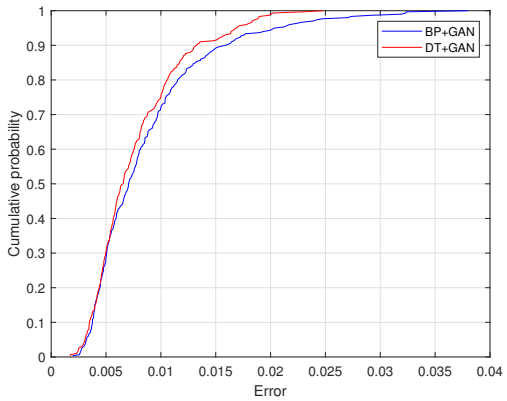

Fig. 10. CDFs of reconstruction error for digits with circles.

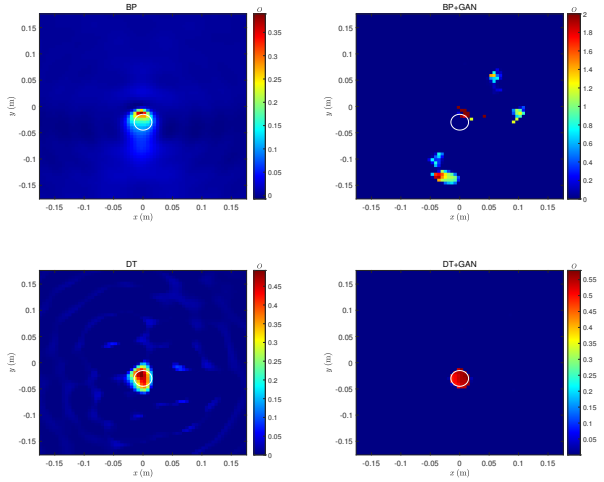

Fig. 11. Reconstruction results using the experimental data (from data set "dielTM_dec8f.exp" at 4 GHz [27]).

under a limited viewing angle, we restrict the rotation angle to the range of 40° to 140° using measurements from the "dielTM_dec8f.exp" dataset at a frequency of 4 GHz.

The neural networks trained in the first test were utilized for verification. Due to alterations in the imaging model and changes in the dimensions of scattering data, the direct application of the GAN method becomes impractical. Fig. 11 illustrates the reconstruction results obtained using BP, DT, BP+GAN, and DT+GAN methods. A white ring on the diagram marks the exact position of the scatterer. Its circular cross-section possesses a radius of 15 mm, with its center positioned at coordinates $(0, -30)$ mm. The estimation of the real part of the relative permittivity yields $\varepsilon_r = 3 \pm 0.3$. The limited observation angle introduces a discrepancy between the BP image and the actual target. Additionally, the imaging model in this scenario significantly deviates from that of the training data, especially concerning the antenna positioning. Specifically, while the excitation wave angle in the training data spans from 0° to 90°, it ranges from 40° to 140° in this case. This substantial difference leads to considerable deviations in the reconstruction outcomes of the BP+GAN technique. However, by employing data extrapolation technology, the DT algorithm can still effectively capture the orientation and size information of scatterers under challenging imaging conditions. Moreover, integrating GAN into DT-based reconstructions (DT+GAN) not only improves the reconstruction accuracy of scatterers but also reduces surrounding artifacts.

Experiments demonstrate that integrating physical priors significantly alleviates the core challenges in deep learning. Specifically, DT's rapid initial estimates reduce reliance on large-scale training data; data extrapolation and prior constraints improve generalizability under narrow observation angles; and adversarial training, guided by physics-informed interactions between the generator and discriminator, effectively suppresses non-physical solutions.

V. CONCLUSION

This paper proposes a hybrid electromagnetic reconstruction algorithm that combines DT and GAN to address the limited viewing angle problem in electromagnetic imaging. This algorithm achieves greater accuracy in reconstructing the scatterer's position, contour, and contrast than the complete learning reconstruction method. This improvement can be attributed to the incorporation of physical mechanisms that effectively reduce the learning complexity of neural networks. Furthermore, compared to other two-step methods like the BP+GAN approach, this algorithm achieves higher solving efficiency by utilizing the fast Fourier transform. Additionally, the introduction of data extrapolation technology effectively addresses reconstruction challenges arising from limited viewing angles. Future research will continue to leverage physical mechanisms to address the inherent nonlinearity and challenges in the mapping process, while extending validation to a wider variety of scatterer geometries, such as multilayered structures, and a more diverse range of observation angles, thereby further evaluating the generalization capabilities.

REFERENCES

[1] Z. Wei and X. Chen, "Solving Full-Wave Nonlinear Inverse Scattering Problems by Deep Learning Schemes," in *2019 IEEE International Conference on Computational Electromagnetics (ICCEM)*, pp. 1-2, IEEE, 2019.

[2] L. Li, L. G. Wang, F. L. Teixeira, C. Liu, A. Nehorai, and T. J. Cui, "DeepNIS: Deep neural network for nonlinear electromagnetic inverse scattering," *IEEE Transactions on Antennas and Propagation*, vol. 67, no. 3, pp. 1819-1825, 2018.

[3] X. Chen, Z. Wei, L. Maokun, P. Rocca, et al., "A review of deep learning approaches for inverse scattering problems (invited review)," *Electromagnetic Waves*, vol. 167, pp. 67-81, 2020.

[4] R. Guo, X. Song, M. Li, F. Yang, S. Xu, and A. Abubakar, "Supervised Descent Learning Technique for 2-D Microwave Imaging," *IEEE Transactions on Antennas and Propagation*, vol. 67, no. 5, pp. 3550-3554, 2019.

[5] G. Chen, P. Shah, J. Stang, and M. Moghaddam, "Learning-Assisted Multimodality Dielectric Imaging," *IEEE Transactions on Antennas*

and Propagation, vol. 68, no. 3, pp. 2356-2369, 2020.

[6] Y. Sanghvi, Y. Kalepu, and U. K. Khankhoje, "Embedding Deep Learning in Inverse Scattering Problems," *IEEE Transactions on Computational Imaging*, vol. 6, pp. 46-56, 2020.

[7] R. Guo, T. Huang, M. Li, H. Zhang, and Y. C. Eldar, "Physics-Embedded Machine Learning for Electromagnetic Data Imaging: Examining three types of data-driven imaging methods," *IEEE Signal Processing Magazine*, vol. 40, no. 2, pp. 18-31, 2023.

[8] K. Xu, Z. Qian, Y. Zhong, J. Su, H. Gao, and W. Li, "Learning-Assisted Inversion for Solving Nonlinear Inverse Scattering Problem," *IEEE Transactions on Microwave Theory and Techniques*, vol. 71, no. 6, pp. 2384-2395, 2023.

[9] C. X. Yang, J. J. Meng, S. Wei, and M. S. Tong, "A Dual-input Electromagnetic Inverse Scattering Algorithm Based on Improved U-net," *Applied Computational Electromagnetics Society Journal (ACES)*, pp. 961-969, 2024.

[10] X. Ye, N. Du, D. Yang, X. Yuan, R. Song, S. Sun, and D. Fang, "Application of Generative Adversarial Network-Based Inversion Algorithm in Imaging 2-D Lossy Biaxial Anisotropic Scatterer," *IEEE Transactions on Antennas and Propagation*, vol. 70, no. 9, pp. 8262-8275, 2022.

[11] R. Song, Y. Huang, K. Xu, X. Ye, C. Li, and X. Chen, "Electromagnetic Inverse Scattering With Perceptual Generative Adversarial Networks," *IEEE Transactions on Computational Imaging*, vol. 7, pp. 689-699, 2021.

[12] M. Li, R. Guo, K. Zhang, Z. Lin, F. Yang, S. Xu, X. Chen, A. Massa, and A. Abubakar, "Machine learning in electromagnetics with applications to biomedical imaging: A review," *IEEE Antennas and Propagation Magazine*, vol. 63, no. 3, pp. 39-51, 2021.

[13] Z. Ma, K. Xu, R. Song, C.-F. Wang, and X. Chen, "Learning-Based Fast Electromagnetic Scattering Solver Through Generative Adversarial Network," *IEEE Transactions on Antennas and Propagation*, vol. 69, no. 4, pp. 2194-2208, 2021.

[14] T. Negishi, V. Picco, L. L. Monte, and D. Erricolo, "Dyadic contrast function for the forward model of diffraction tomography of thin cylindrical objects," *IEEE Antennas and Wireless Propagation Letters*, vol. 16, pp. 991-994, 2016.

[15] C. Yang, J. Zhang, and M. S. Tong, "An FFT-accelerated particle swarm optimization method for solving far-field inverse scattering problems," *IEEE Transactions on Antennas and Propagation*, vol. 69, no. 2, pp. 1078-1093, 2020.

[16] A. Aggarwal, M. Mittal, and G. Battineni, "Generative adversarial network: An overview of theory and applications," *International Journal of Information Management Data Insights*, vol. 1, no. 1, p. 100004, 2021.

[17] L. Guo, G. Song, and H. Wu, "Complex-valued Pix2pix—Deep neural network for nonlinear electromagnetic inverse scattering," *Electronics*, vol. 10, no. 6, p. 752, 2021.

[18] C. Yang, J. Zhang, and M. Tong, "A novel diffraction tomographic algorithm with narrow observation angle," *International Journal of Numerical Modelling: Electronic Networks, Devices and Fields*, vol. 32, no. 5, p. e2583, 2019.

[19] W. C. Chew, *Waves and Fields in Inhomogenous Media*, vol. 16, John Wiley & Sons, 1999.

[20] K. Belkebir, P. C. Chaumet, and A. Sentenac, "Superresolution in total internal reflection tomography," *J. Opt. Soc. Am. A*, vol. 22, no. 9, pp. 1889-1897, Sep. 2005.

[21] Z. Wei and X. Chen, "Deep-learning schemes for full-wave nonlinear inverse scattering problems," *IEEE Transactions on Geoscience and Remote Sensing*, vol. 57, no. 4, pp. 1849-1860, 2018.

[22] I. Goodfellow, J. Pouget-Abadie, M. Mirza, B. Xu, D. Warde-Farley, S. Ozair, A. Courville, and Y. Bengio, "Generative adversarial networks," *Communications of the ACM*, vol. 63, no. 11, pp. 139-144, 2020.

[23] S. Woo, J. Park, J.-Y. Lee, and I. S. Kweon, "CBAM: Convolutional Block Attention Module," in *Proceedings of the European Conference on Computer Vision (ECCV)*, Sep. 2018.

[24] O. Ronneberger, P. Fischer, and T. Brox, "U-Net: Convolutional Networks for Biomedical Image Segmentation," in N. Navab, J. Hornegger, W. M. Wells, and A. F. Frangi, editors, *Medical Image Computing and Computer-Assisted Intervention – MICCAI 2015*, pp. 234-241, Springer International Publishing, Cham, 2015.

[25] C. X. Yang, J. Zhang, and M. S. Tong, "A hybrid inversion method based on the bat algorithm for microwave imaging of two-dimensional dielectric scatterers," *Progress in Electromagnetics Research M*, vol. 102, pp. 91-104, 2021.

[26] Y. Lecun, L. Bottou, Y. Bengio, and P. Haffner, "Gradient-based learning applied to document recognition," *Proceedings of the IEEE*, vol. 86, no. 11, pp. 2278-2324, 1998.

[27] K. Belkebir and M. Saillard, "Testing inversion algorithms against experimental data," *Inverse problems*, vol. 17, no. 6, p. 1565, 2001.

Chun Xia Yang received the Ph.D. degree in electronic science and technology from Tongji University, Shanghai, China, in 2017. During her doctoral studies, she also conducted research at the Department of Electrical and Computer Engineering, University of Illinois at Urbana-Champaign, Champaign, IL, USA as a visiting student between 2014 and 2016. She is currently an associate professor at the Department of Communication Engineering, Shanghai Normal University, Shanghai, China. Her ongoing research interests primarily revolve around electromagnetic inverse scattering for imaging and computational electromagnetics.

Xirui Yang received her B.S. degree in Communication Engineering and M.S. degree in Electronic Information from Shanghai Normal University, Shanghai, China, in 2021 and 2024, respectively. She is currently affiliated with the School of Electronic and Information Engineering, Guangzhou City University of Technology, Guangzhou, China. Her research focuses primarily on electromagnetic inverse scattering.

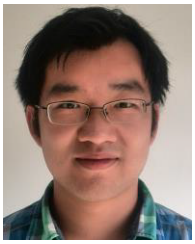

Jian Zhang received his B.S. degree in Electronics Science and Technology and his Ph.D. degree in Control Science and Engineering from Tongji University, Shanghai, China, in 2014 and 2020, respectively. He is currently working as an Engineer at Xpeedic Technology, Inc., Shanghai, China. His research mainly focuses on multi-physics numerical simulation techniques.

Chi Zhou received the M.S. degree in Electronic Information from Shanghai Normal University, Shanghai, China, in 2025. He is currently affiliated with Wenyin Cloud Computing Co., Ltd, Shanghai, China. His research mainly focuses on electromagnetic inverse scattering.

Mei Song Tong received the B.S. and M.S. Degrees from Huazhong University of Science and Technology, Wuhan, China, respectively, and Ph.D. degree from Arizona State University, Tempe, Arizona, USA, all in electrical engineering. He is currently the Distinguished Professor and Head of Department of Electronic Science and Technology, and Vice Dean of College of Microelectronics, Tongji University, Shanghai, China. He has also held an adjunct professorship at the University of Illinois at Urbana-Champaign, Urbana, Illinois, USA, and an honorary professorship at the University of Hong Kong, China. He has published more than 700 papers in refereed journals and conference proceedings and coauthored six books or book chapters. His research interests include electromagnetic field theory, antenna theory and design, simulation and design of RF/microwave circuits and devices, interconnect and packaging analysis, inverse electromagnetic scattering for imaging, and computational electromagnetics.

Prof. Tong is a Fellow of the Electromagnetics Academy, Fellow of the Japan Society for the Promotion of Science (JSPS), and Senior Member (Commission B) of the USNC/URSI. He has been the chair of Shanghai Chapter since 2014 and the chair of SIGHT committee in 2018, respectively, in IEEE Antennas and Propagation Society. He has served as an associate editor or guest editor for several well-known international journals, including IEEE Antennas and Propagation Magazine, IEEE Transactions on Antennas and Propagation, IEEE Transactions on Components, Packaging and Manufacturing Technology, International Journal of Numerical Modeling: Electronic Networks, Devices and Fields, Progress in Electromagnetics Research, and Journal of Electromagnetic Waves and Applications, etc. He also frequently served as a session organizer/chair, technical program committee member/chair, and general chair for some prestigious international conferences. He was the recipient of a Visiting Professorship Award from Kyoto University, Japan, in 2012, and from University of Hong Kong, China, 2013. He advised and coauthored 15 papers that received the Best Student Paper Award from different international conferences. He was the recipient of the Travel Fellowship Award of USNC/URSI for the 31th General Assembly and Scientific Symposium (GASS) in 2014, Advance Award of Science and Technology of Shanghai Municipal Government in 2015, Fellowship Award of JSPS in 2016, Innovation Award of Universities' Achievements of Ministry of

Education of China in 2017, Innovation Achievement Award of Industry-Academia-Research Collaboration of China in 2019, "Jinqiao" Award of Technology Market Association of China in 2020, Baosteel Education Award of China in 2021, Carl Friedrich von Siemens Research Award of the Alexander von Humboldt Foundation of Germany in 2023, and Technical Achievement Award of Applied Computational Electromagnetic Society (ACES) of USA in 2024. In 2018, he was selected as the Distinguished Lecturer (DL) of IEEE Antennas and Propagation Society for 2019-2022.